

Supporting Information

Experimental section

Materials. Graphite powder (200 mesh, 99.9999%) was purchased from Alfa Aesar Co., Ltd, United States. Ammonium hydroxide ($\text{NH}_3 \cdot \text{H}_2\text{O}$, 28%), glacial acetic acid, methylene chloride (CH_2Cl_2), petroleum ether were purchased from GENERAL-REAGENT, Titan Scientific Co., Ltd, Shanghai, China. 3,4-Ethylenedioxythiophene (EDOT), N-bromosuccinimide (NBS) were purchased from Adamas-beta, Titan Scientific Co., Ltd, Shanghai, China. Concentrated sulfuric acid (H_2SO_4 , 98%), potassium permanganate (KMnO_4), hydrogen peroxide (H_2O_2 , 30%) and chloroform were given by Prof. W. Dong, Nanjing University of Science & Technology, China. Distilled water was obtained from Direct-Q3 UV, Millipore.

Synthesis and purification of graphene oxide (GO). Graphite oxide was synthesized by a modified Hummers method firstly. In brief, 2.0 g of graphite was first mixed in a solution of 100.0 ml of H_2SO_4 in an ice bath for 3 hours. Then, 8.0 g of KMnO_4 was slowly added into the solution. After it was stirred for 2 hours, 200.0 ml of distilled water was added drop by drop under ordinary temperature water bath. After additional 30 minutes stirring, 10.0 ml of H_2O_2 was added slowly into the above-mentioned solution, and a bright yellow of graphite oxide appearance during this process. The graphite oxide was filtered and washed by

distilled water for 4 times to remove all the impurity. Then, the gel like graphite oxide was freeze-dried at $-50\text{ }^{\circ}\text{C}$ for 24 hours to obtain graphite oxide powder. The graphite oxide powder was dispersed in distilled water as 1 mg ml^{-1} , and centrifuged at $10000\text{ rap min}^{-1}$ for 30 minutes to remove all the agglomerate sheets. And the GO was obtained at supernatant and dried at $50\text{ }^{\circ}\text{C}$.

Synthesis of 3D-reduced GO (3D-RGO). 0.7 ml of $\text{NH}_3\cdot\text{H}_2\text{O}$ was added into 60.0 ml of GO solution (1.5 mg ml^{-1} , in water), followed by sonication for 10 minutes. The dark brown colloidal dispersion was sealed in a 100-ml Teflon-lined autoclave and maintained at $180\text{ }^{\circ}\text{C}$ for 12 hours. Then the autoclave was naturally cooled to room temperature and the as-prepared 3D-RGO was taken out and subsequently freeze-dried for 24 hours to obtain 3D-RGO.

Synthesis of 2,5-dibromo-3,4-ethylenedioxythiophene (DBEDOT). 2,5-Dibromo-3,4-ethylenedioxythiophene (DBEDOT) monomer was synthesized according to the previous reports with minor modifications.^{1,2} In brief, 6.0 g of EDOT was first mixed in a solution of 100.0 ml of CHCl_3 and 100.0 ml of glacial acetic acid. Then, 16.0 g of NBS was slowly added into the above-mentioned solution at $0\text{-}5\text{ }^{\circ}\text{C}$ under an Ar atmosphere. After it was stirred for 5 hours, the solution was then poured into 200 mL of distilled water. The green-blue organic layer was separated, and the water layer was extracted with CHCl_3 ($50\text{ mL} \times 3$).

The combined organic layer was washed with distilled water for several times. The solvent was then removed under vacuum by rotary evaporation. The dark blue solid product was purified using column chromatography with CH₂Cl₂ and petroleum ether (1:1) as eluent to get white crystals in 75% yield (9.5 g). ¹H NMR (CDCl₃): (4.4 ppm, s, CH₂). ¹³C NMR (CDCl₃): 140.3, 84.6, 65.1 ppm.

Synthesis of self-assembly 3D-RGO/PEDOT architecture. 53.3 mg of 3D-RGO was added into 100.0 ml of DBEDOT solution (100.0 mg ml⁻¹ in CHCl₃). After absorption for 1 hour, the architecture was moved out and heating at 70 °C for 4 hours. The solvent would be released to the atmosphere and the DBEDOT would be solid-state polymerized in the 3D architecture's pores. The obtained self-assembly 3D-RGO/PEDOT architecture is 227.6 mg.

Characterization and measurement. The detailed morphologies of the 3D-RGO, 3D-RGO/PEDOT, DBEDOT and SSP PEDOT were observed with a field emission scanning electron microscope (FE-SEM, S4800, Hitachi). Contact angle was carried out in a Mingyu MY-SPCX1 contact angle measurement. Fourier transform infrared (FTIR) spectra were recorded on a Varian 670-IR. X-ray photoelectron spectra (XPS) was carried out in a Thermo Scientific ESCALAB 250Xi X-ray photoelectron spectrometer equipped with a monochromatic Al K α X-ray source (1486.6 eV). Raman spectroscopy was carried out on a Renishaw in Via

Raman Microscope, equipped with 532 nm laser. Electromagnetic measurements used an Agilent N5242A PNA-X vector network analyzer in the frequency range of 2-18 GHz. The measured samples were prepared by uniformly mixing 10 wt% of the sample with a paraffin matrix at 100 °C. The mixture was then pressed into toroidal shaped samples with an outer diameter of 7.00 mm and inner diameter of 3.04 mm. In a coaxial wire analysis, a radiated wave undergoes shielding (reflection, absorption, and transmission) when the incident wave at a point i pass toward another point j, and these wave scattering values are expressed as S_{ji} . To probe further, ϵ_r of the dielectric material has been calculated from the experimental scattering parameters S_{11} (or S_{22}) and S_{21} (or S_{12}) using the standard Nicolson-Ross-Weir (NRW) algorithm.^{3,4} Differential scanning calorimetry (DSC) was run on a DSC 823e (Mettler Toledo) with a heating rate of 10 °C/min under a nitrogen flow.

Theory of electromagnetic absorption

Due to the frequency range is from 2-18 GHz, the source-to-shield distance be greater than the free-space wavelength, so the measurements are considered under far field.⁵ According to the transmission line theory,⁶ the input impedance (Z_{in}) on the interface can be expressed as

$$Z_m = Z_0 \sqrt{\frac{\mu_r}{\epsilon_r}} \tanh\left(j \frac{2\pi f d}{c} \sqrt{\epsilon_r \mu_r}\right) \quad (1)$$

Where Z_0 is the impedance of free space, μ_r is the complex permeability, $\mu_r = \mu' - j\mu''$, ϵ_r is the complex permittivity, $\epsilon_r = \epsilon' - j\epsilon''$, f is the frequency,

d is the thickness of material, c is the speed of light.

So the reflection loss (RL) can be expressed as

$$RL(dB) = 20 \lg \left| \frac{Z_{in} - Z_0}{Z_{in} + Z_0} \right| \quad (2)$$

Morphologies of DBEDOT and PEDOT

Fig. S1 gives the significant change of the surface morphology. The pure DBEDOT has a smooth surface, but the surface of the PEDOT film exhibits a stripe-like microstructure which might result from the formation of the polymer chain during the polymerization process.^{1,7} And this morphology of PEDOT is also find in 3D-RGO/PEDOT (Fig. 2g).

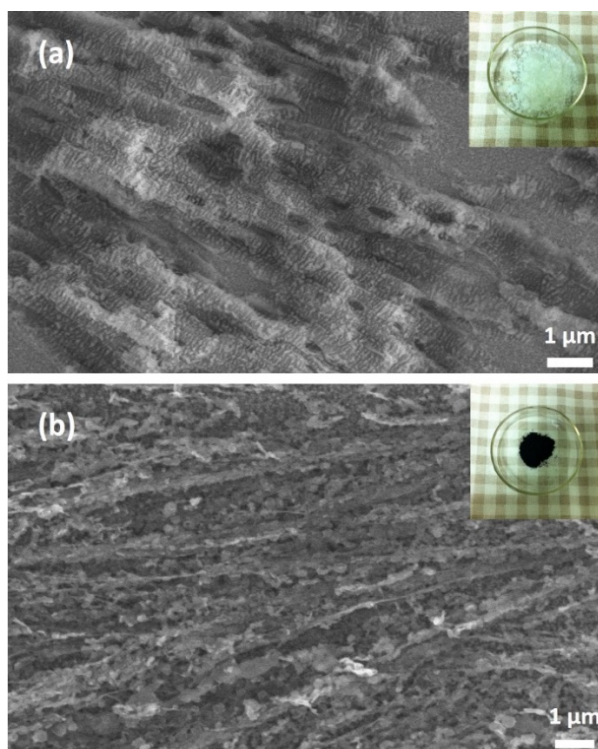


Fig. S1 Digital photos and FE-SEM images of DBEDOT (a) and SSP PEDOT (b)

DSC analysis of DBEDOT

It gives an endothermic melting phenomenon, when heating the monomer DBEDOT at 10 °C/min. As we can find from Fig. S2, the position of the melting peak is at 97.65 °C. The melting point results in an exothermic polymerization peak at 135.23 °C, which means the polymer formation, and doping.¹ Additionally, it is a quite suitable temperature (70 °C) for SSP, which we have chosen in this experiment.

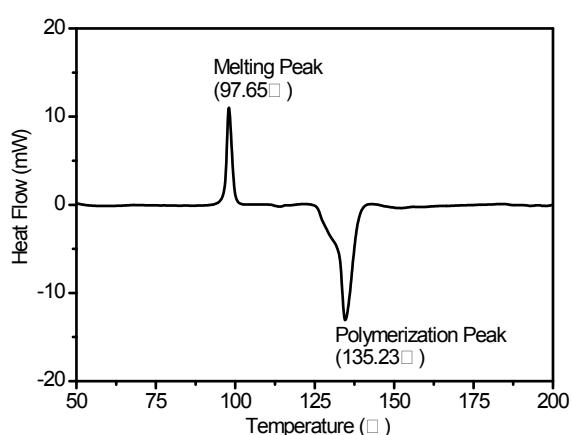


Fig. S2 DSC curves of the DBEDOT at the heating scan of 10 °C/min under nitrogen flow.

Detail morphology of 3D-RGO/PEDOT

In Fig. S3, more evidences that DBEDOT had been SSP in 3D-RGO's pores was found under high-resolution FE-SEM images. The SSP-PEDOT can be found in the micrometers pores area, rather than dispersed on RGO skeleton surface.

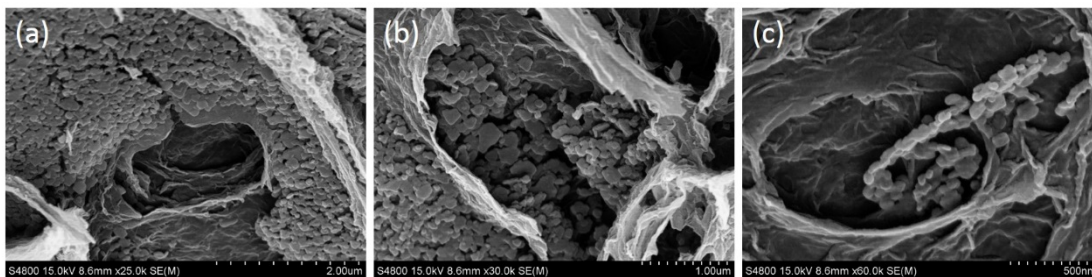


Fig. S3 FE-SEM images of 3D-RGO/PEDOT with high-resolution.

FTIR analysis of 3D-RGO/PEDOT

Fig. S4 shows that the peaks about 1506.1 and 1351.9 cm^{-1} are ascribed to the C=C/C-C stretching of the thiophene rings, and the peaks at 1196.9 and 1075.7 cm^{-1} are ascribed to the C-O-C stretching.⁸ Furthermore, the peaks at 974.8 and 838.0 cm^{-1} are ascribed to the oxyethylene ring stretching and the peak at around 694.1 is attributed to the symmetric C-S-C stretching in the thiophene ring, respectively.⁹ These series evidences indicate that SSP-PEDOT is successfully grown into 3D-RGO's pores.

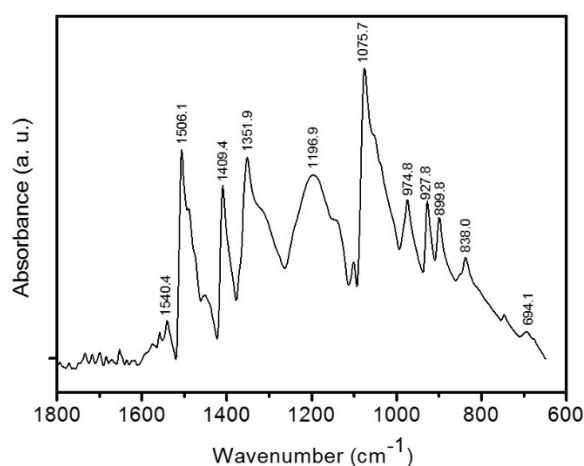


Fig. S4 FTIR spectrum of 3D-RGO/PEDOT.

XPS analysis of GO, 3D-RGO and 3D-RGO/PEDOT

In Fig. S5, the survey XPS spectrum of 3D-RGO/PEDOT has been given. The element of Br, S, C, and O has been characterized which was complied with the content element of 3D-RGO/PEDOT. There are four types of carbon bonds, include C–C (284.8 eV), C–O (286.6 eV), C=O (288.0 eV), and O–C=O (289.2 eV) in C 1s XPS spectrum of GO,¹⁰ indicate that GO has been highly oxidized (Fig. S6a). Although the C 1s XPS spectrum of 3D-RGO also has some oxygenated groups, but they are much weaker than GO (Fig. S6b). When DBEDOT was absorbed into 3D-RGO and polymerized to form PEDOT, a new peak centered at 285.3 eV (Fig. S6c), which was attributed to C–S bond in PEDOT.⁸

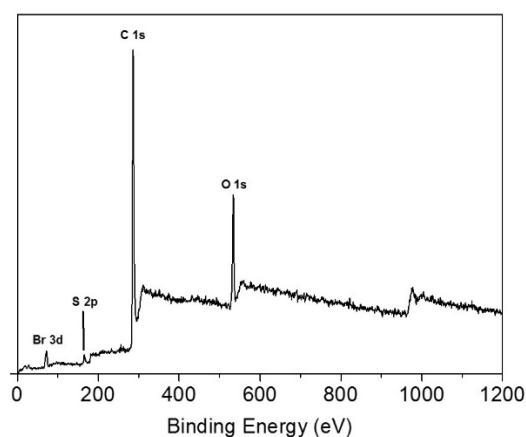


Fig. S5 Survey XPS spectrum of 3D-RGO/PEDOT.

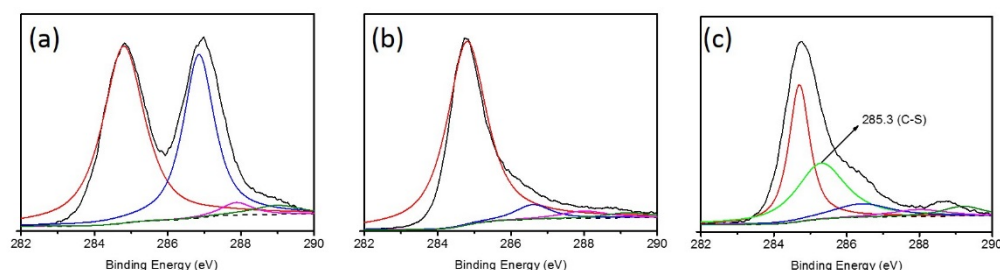


Fig. S6 C 1s XPS spectrum of GO (a), 3D-RGO (b), and 3D-

RGO/PEDOT (c).

Raman analysis of GO, 3D-RGO, and 3D-RGO/PEDOT

In Fig. S7, the Raman spectrums of GO, 3D-RGO, and 3D-RGO/PEDOT are associated with a typical D band and G band around 1347 cm^{-1} and 1581 cm^{-1} respectively. The D band is due to the breathing mode of κ -point photons of A_{1g} symmetry and the G band arises from the first-order scattering of E_{2g} phonons by sp^2 carbon atoms.^{11,12} During the hydrothermal reduction process, although the oxygen group has been removed from the carbon layer, but the defect in carbon lattice structure has been aroused, let the value of I_D/I_G increased from 1.62 to 1.93. When the PEDOT was polymerized in 3D-RGO's pores, the value of I_D/I_G further increased to 2.12. This phenomenon should be attribute to the contribution of sp^3 structure in SSP-PEDOT.

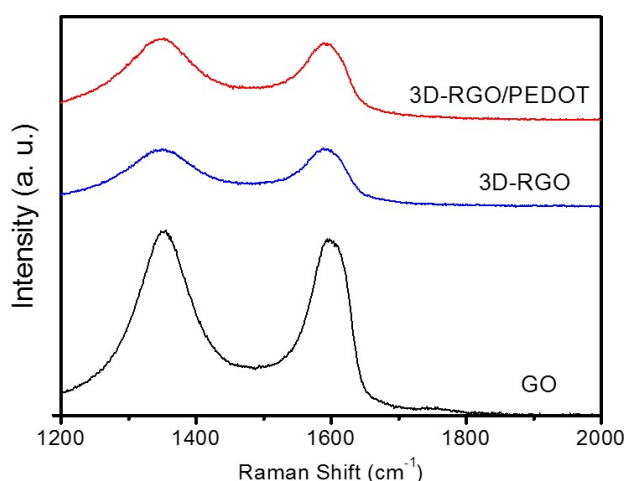


Fig. S7 Raman spectrum of GO, 3D-RGO, and 3D-RGO/PEDOT.

Dielectric and electromagnetic absorption analysis.

The permittivity of each sample was measured using coaxial wire

method.[] Fig. S8 shows the ϵ' and ϵ'' measured in the frequency range of 2-18 GHz for each sample. As shown in Fig. S8a, the values of ϵ' nearly decrease with increasing frequency in each sample, which may be related to a resonance behavior that was reported before.¹³ The values of ϵ'' keep stable relatively in 3D-RGO/PEDOT (Fig. S8b), however, the total tendency of the values of ϵ'' in 3D-RGO is decreasing gradually. Nevertheless, the values of ϵ'' in 3D-RGO are larger than two samples of 3D-RGO/PEDOT in the whole frequency range. The $\tan\delta = \epsilon''/\epsilon'$, where δ is the dielectric loss angle of the material. Energy loss in a material illuminated by electromagnetic waves comes about through damping forces acting on polarized atoms and molecules and through the finite conductivity of a material. Due to the contribution of large ϵ'' in 3D-RGO, it has much larger values of $\tan\delta$ than 3D-RGO/PEDOT (Fig.S9a). Due to ϵ'' is a measure of dielectric losses, it is easy to accept that large ϵ'' should bring strong electromagnetic absorption. However, in a composite filled with dielectric particles only, at the best matching condition, the maximum RL as follows:¹⁴

$$RL_{max} = 20lg \left| \frac{\frac{1}{\epsilon} - 1}{\frac{1}{\epsilon} + 1} \right| \quad (3)$$

after some transformation, we obtain

$$RL_{max} = 20 \lg \left(1 - \frac{4}{2 + \varepsilon'' \left(\tan \delta + \frac{1}{\tan \delta} \right)} \right) \quad (4)$$

thus, maximum RL should be evaluated by considering both ε'' and dielectric loss tangent ($\tan \delta$). This is further confirmed by the attenuation constant (α),¹⁴

$$\alpha = \frac{\omega}{\sqrt{2c}} \sqrt{-\varepsilon' + \sqrt{(\varepsilon')^2 + \varepsilon''^2}} \quad (5)$$

after some transformation and matching frequency, α reads as,

$$\alpha = \frac{\omega}{\sqrt{2d}} \sqrt{\frac{1}{\varepsilon''} \left(\sqrt{1 + \frac{1}{\tan^2 \delta} - \frac{1}{\tan \delta}} \right)} \quad (6)$$

In Fig S9b, the values of α with each sample has been shown. It is imply that 3D-RGO/PEDOT has better electromagnetic absorption performance due to the large values of α .

We consider that Debye dipolar relaxation is an important mechanism by which dielectric absorption materials absorb electromagnetic radiation. The relative complex permittivity can be expressed by the following equation:¹⁵

$$\varepsilon_r = \varepsilon_\infty + \frac{\varepsilon_s - \varepsilon_\infty}{1 + j2\pi f\tau} \quad (7)$$

Where f , ε_s , ε_∞ , and τ are the frequency, static permittivity, relative dielectric permittivity at the high-frequency limit, and polarization relaxation time, respectively. Thus, ε' and ε'' can be described by

$$\varepsilon' = \varepsilon_{\infty} + \frac{\varepsilon_s - \varepsilon_{\infty}}{1 + (2\pi f)^2 \tau^2} \quad (8)$$

$$\varepsilon'' = \frac{2\pi f \tau (\varepsilon_s - \varepsilon_{\infty})}{1 + (2\pi f)^2 \tau^2} \quad (9)$$

According to (8) and (9), the relationship between ε' and ε'' can be expressed:

$$\left(\varepsilon' - \frac{\varepsilon_s - \varepsilon_{\infty}}{2}\right)^2 + (\varepsilon'')^2 = \left(\frac{\varepsilon_s - \varepsilon_{\infty}}{2}\right)^2 \quad (10)$$

Thus, the plot of ε' versus ε'' would be a single semicircle, generally denoted as the Cole-Cole semicircle. It can be seen in Fig. S10 that the curves of 3D-RGO and 3D-RGO/PEDOT have the same general shape, this suggests that there are quadruple relaxation process, representing the contribution of Debye relaxation,¹⁶ and this relaxation processes are usually caused by a delay in molecular polarization with respect to a changing electric field in a dielectric medium.¹⁵

As shown in Fig. S11, 3D-RGO has a poor electromagnetic absorption properties in the whole frequency range both in low and high thickness, this phenomenon also reported by former works,¹⁷ and it also can explain that too large ε'' will not be in favor of absorption. Although, SSP PEDOT can get an effective range deeper than -10 dB about 5.9 GHz with 2.0 mm of thickness, but it need a very high content (50 wt%) in composites. The reason why self-assembly 3D-RGO/PEDOT has an excellent electromagnetic absorption properties, should be contributed to the pore structure improve the contact surface between electromagnetic

wave and PEDOT.

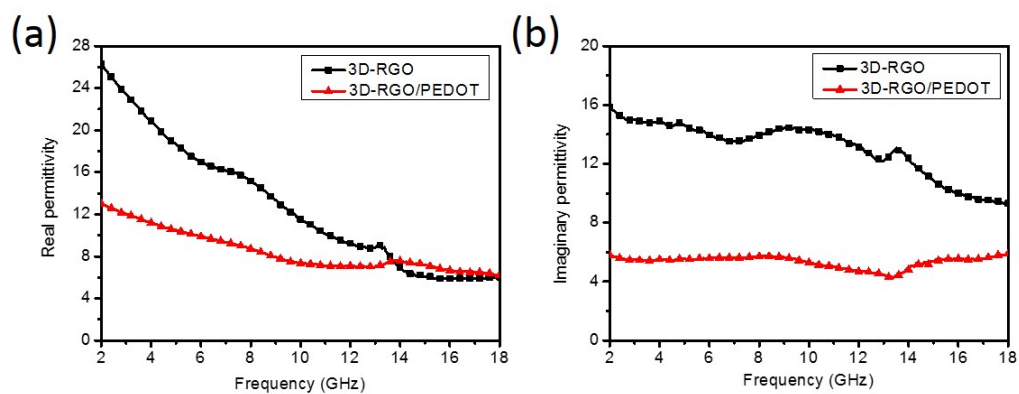


Fig. S8 Real part (a) and imaginary part (b) of relative complex permittivity of 3D-RGO and 3D-RGO/PEDOT.

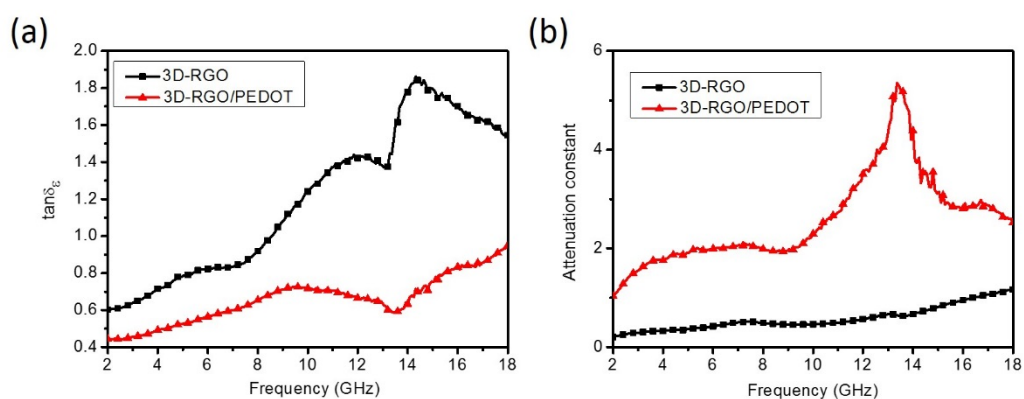


Fig. S9 Dielectric loss tangent (a) and attenuation constant (b) of 3D-RGO and 3D-RGO/PEDOT.

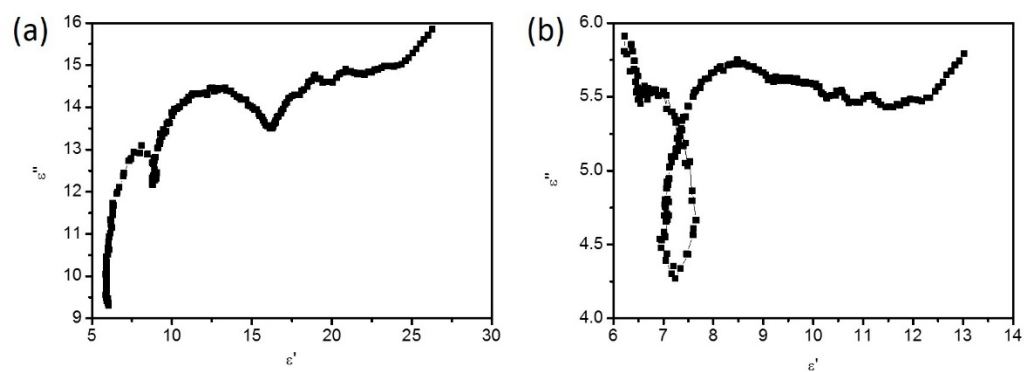


Fig. S10 ϵ' - ϵ'' curves of 3D-RGO (a) and 3D-RGO/PEDOT (b) mixing with paraffin by 10 wt%.

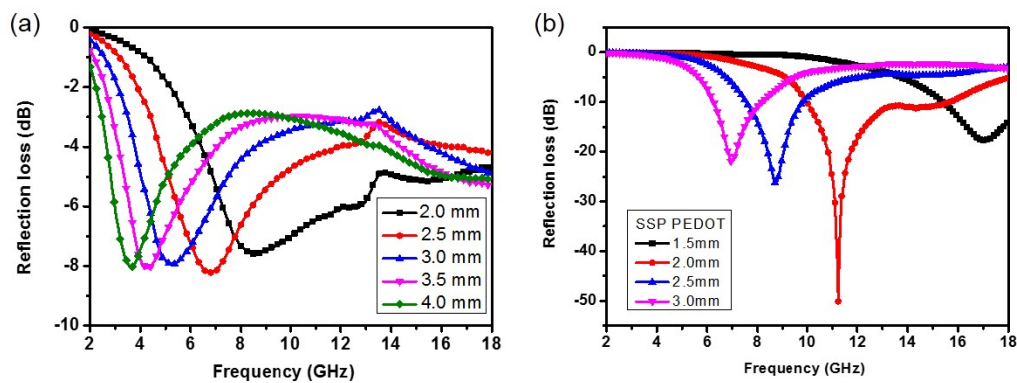


Fig. S11 Reflection loss curves for samples of 3D-RGO (10 wt% mixing with paraffin) with different thicknesses (2.0 to 4.0 mm) (a) and SSP PEDOT (50 wt% mixing with paraffin) with different thicknesses (1.5 to 3.0 mm) (b).

Notes and references

- 1 H. Meng, D. F. Perepichka, M. Bendikov, F. Wudl, G. Z. Pan, W. J. Yu, W. J. Dong and S. Brown, *J. Am. Chem. Soc.*, 2003, **125**, 15151.
- 2 G. A. Sotzing, J. R. Reynolds and P. J. Steel, *Chem. Mater.*, 1996, **8**, 882.
- 3 A. M. Nicolson and G. F. Ross, *IEEE Trans. Instrum. Meas.*, 1970, **4**, 377.
- 4 W. B. Weir, *Proc. IEEE*, 1974, **62**, 33.
- 5 N. F. Colaneri and L. W. Shacklette, *IEEE Trans. Instrum. Meas.*, 1992, **41**, 291.

- 6 Y. Naito and K. Suetake, *IEEE Trans. Microwave Theory*, 1971, **19**, 65.
- 7 H. Meng, D. F. Perepichka, and F. Wudl, *Angew. Chem., Int. Ed.*, 2003, **42**, 658.
- 8 P. B. Liu, Y. Huang and X. Sun, *ACS Appl. Mater. Interfaces*, 2013, **5**, 12355.
- 9 F. Alvi, M. K. Ram, P. A. Basnayakab, E. Stefanakosa, Y. Goswamid, and A. Kuarb, *Electrochim. Acta*, 2011, **56**, 9406.
- 10 Y. X. Xu, K. X. Sheng, C. Li and G. Q. Shi, *ACS Nano*, 2010, **4**, 4324.
- 11 Z. Jin, J. Yao, C. Kittrell, and J. M. Tour, *ACS Nano*, 2011, **5**, 4112.
- 12 W. F. Chen, S. R. Li, C. H. Chen, and L. F. Yan, *Adv. Mater.* 2011, **23**, 5679.
- 13 H. Zhang, A. J. Xie, C. P. Wang, H. S. Wang, Y. H. Shen, X. Y. Tian, *J. Mater. Chem. A*, 2013, **1**, 8547.
- 14 F. Qin and C. Brosseau, *J. Appl. Phys.*, 2012, **111**, 061301.
- 15 S. He, G. S. Wang, C. Lu, J. Liu, B. Wen, H. Liu, L. Guo and M. S. Cao, *J. Mater. Chem. A*, 2013, **1**, 4685.
- 16 D. Chen, G. S. Wang, S. He, J. Liu, L. Guo and M. S. Cao, *J. Mater. Chem. A*, 2013, **1**, 5996.
- 17 C. G. Hu, Z. Y. Mou, G. W. Lu, N. Chen, Z. L. Dong, M. J. Hu and L .T. Qu, *Phys. Chem. Chem. Phys.*, 2013, **15**, 13038.